Inorganic Chemistry

Article

pubs.acs.org/IC

Synthesis of Functionalized Materials Using Aryloxo-Organometallic Compounds toward Spinel-like MM'_2O_4 ($M = Ba^{2+}$, Sr^{2+}; $M' = In^{3+}$, Al^{3+}) Double Oxides

Łukasz John,[†] Magdalena Kosińska-Klähn,[†] Lucjan B. Jerzykiewicz,[†] Leszek Kępiński,[‡] and Piotr Sobota*[,†]

[†]Faculty of Chemistry, University of Wrocław, F. Joliot-Curie 14, 50-383 Wrocław, Poland

[‡]Institute of Low Temperature and Structural Researches, Polish Academy of Sciences in Wrocław, 2 Okólna, 50-422 Wrocław, Poland

Supporting Information

ABSTRACT: The predesigned single-source precursors [Ba{(μ-ddbfo)$_2$InMe$_2$}$_2$] (**1**), [Me$_2$In(μ-ddbfo)]$_2$ (**2**), [Sr{(μ-ddbfo)$_2$AlMe$_2$}$_2$] (**4**), and [Me$_2$Al(μ-ddbfo)]$_2$ (**5**) (ddbfoH = 2,3-dihydro-2,2-dimethylbenzofuran-7-ol) for spinel-like double oxides and group 13 oxide materials were prepared via the direct reaction of the homoleptic aryloxide [M(ddbfoH)$_4$]-(ddbfo)$_2$·ddbfoH (M = Ba^{2+}, Sr^{2+} (**3**)) and InMe$_3$ or AlMe$_3$ in toluene. In all of the reactions, there was an organometallic-driven abstraction of the OH protons from the 7-benzofuranols in the Ba^{2+} and Sr^{2+} cation sphere. All compounds were characterized by elemental analysis, ^{1}H NMR, and FT-IR spectroscopy. In addition, the molecular structures of **1**, **2**, and **3** were determined by single-crystal X-ray diffraction. The oxide products derived from the compounds mentioned above were studied using elemental analysis, Raman spectroscopy, X-ray powder diffraction, and scanning and transmission electron microscopy equipped with an energy-dispersive spectrometer. Moreover, their specific surface area and mesopore size distribution were evaluated using nitrogen porosimetry. Preliminary investigations of the Eu-doped $SrAl_2O_4$ and In_2O_3 phosphors revealed that the oxides obtained could be considered as matrices for lanthanide ions.

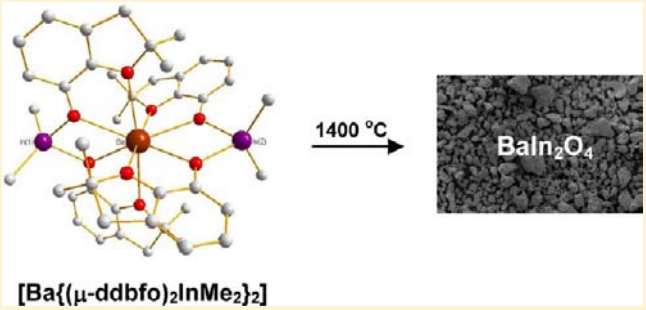

INTRODUCTION

The structure and properties of spinel-like oxides have attracted considerable attention in recent years from both engineers and scientists.[1] These materials possess interesting magnetic and electronic properties[2] and are suitable for numerous technological applications, including magnetic core materials,[3] superconductors,[4,5] high-frequency devices, cathode materials for commercially available batteries,[6] semiconductors,[7] and gas sensors,[8] and they also constitute efficient oxide networks for luminescent materials.[9] Strontium and barium aluminates, for example, represent some of the most studied and efficient host materials for long-lasting phosphorescence, and their synthesis and optical properties have been extensively explored during the past decades.[10−12] Similarly, calcium aluminate has been used as a hydraulic material in the cement industry[13] and also in high-strength and high-toughness ceramic/polymer composites.[14] Group 13 oxides, on the other hand, such as Al_2O_3, Ga_2O_3, and In_2O_3, are important components of spinel materials. For example, indium oxide has been extensively investigated for its semiconducting properties[15] and is commonly used in several microelectronic areas, including window heaters, liquid crystal displays, solar cells,[16] and gas sensors.[17,18] Moreover, the widespread occurrence of Al_2O_3 is strongly emphasized in the industry, where it is used as a catalyst and catalyst support in gas absorption,[19] in lighting as a component of sodium vapor lamps,[20] and in health and medical applications, where it is used as a material in hip replacements.[21] Furthermore, alumina is used as a dosimeter for radiation protection and in other therapeutic applications for its optically stimulated luminescence properties.

In view of the wide range of applications mentioned above for oxides, there is a strong impetus to seek out novel and inexpensive methods for their synthesis. Classically, mixed-cation oxide ceramics are synthesized according to conventional solid-state reactions involving oxides, carbonates, or nitrates at relatively high temperatures (~1500 °C). These procedures are largely inefficient and often lead to inhomogeneous byproduct with poor control over the stoichiometry and phase purity.[22] These disadvantages have led to the rapid development of new preparation techniques involving specific precursors.[23] Metal alkoxides and aryloxides represent a very important group of such precursors, especially those that have strictly defined metal stoichiometries on the molecular level.[24,25] Thus, they already have metal−oxygen bonds established, and their thermal decomposition can be performed at relatively low temperatures in contrast to solid-state reactions. Moreover, oxide ceramics

Received: June 7, 2012
Published: August 29, 2012

   dx.doi.org/10.1021/ic301218v | Inorg. Chem. 2012, 51, 9820−9832

derived from these materials are highly phase-pure and possess specific properties such as high levels of hardness, chemical and mechanical resistance, and thermal stability.[23] As a consequence, these materials are perfect candidates for sol−gel and metal−organic chemical vapor-phase deposition (MOCVD) conversion to the appropriate metal oxides.

Metal alkoxides and aryloxides are almost as common in today's chemistry as any other simple inorganic compounds and represent an enormous family of species with broad structural diversity. In the literature, the population of structurally characterized heterobimetallic complexes of heavier alkaline-earth and group 13 metals is not significantly large.[26] This list includes some alkoxo, alkoxo-hydride, and alkoxo-organo-metallic compounds that constitute so-called single-source precursors (SSPs) for spinel-like double oxides. For example, Veith and co-workers reported the well-defined volatile hydridoalkoxide $[Mg\{(O^tBu)_2AlH_4\}_2]$.[27] Kessler et al. also obtained a new class of heteroleptic divalent metal−aluminum alkoxide complexes $[MAl_2(acac)_3(O^iPr)_4(OAc)]$ (M = Co, Zn; acac = acetylacetone; OAc = acetate).[28] Another example reported in the literature involved a nickel−aluminum $[NiAl_2(acac)_4(O^iPr)_4]$ compound.[29] In our research group, we have also obtained some calcium−[30] and barium−aluminum, barium−gallium,[31] and group 2/group 4 alkoxo- and aryloxo-organometallic compounds, which are perfect candidates for double oxides.[32−34] We have shown that coordinated alcohol molecules that possess a hydroxyl group at the metal site are perfect anchors for organometallic moieties because they bring metal atoms close to one another and have a fixed ratio for metals depending on the oxide used.[35] The driving force for this reaction was the organometallic-driven abstraction of the hydroxyl protons from the alcohol groups attached to the metal sphere. During the initial phases of our approach, we were interested in using the valuable features of barium and strontium aryloxides $[M(ddbfoH)_4](ddbfo)_2{\cdot}ddbfoH$ (M = Ba^{2+},[36] Sr^{2+} (**3**)). Herein, we report the results of our recent studies involving the synthesis of a series of novel aryloxo-organometallics, including barium−indium $[Ba\{(\mu\text{-}ddbfo)_2InMe_2\}_2]$ (**1**), indium $[Me_2In(\mu\text{-}ddbfo)]_2$ (**2**), strontium−aluminum $[Sr\{(\mu\text{-}ddbfo)_2AlMe_2\}_2]$ (**4**), and aluminum $[Me_2Al(\mu\text{-}ddbfo)]_2$ (**5**) complexes (ddbfoH = 2,3-dihydro-2,2-dimethylbenzofuran-7-ol). Such an approach allowed for the construction of compounds possessing the predesigned molecular structure for the generation of $BaIn_2O_4$, In_2O_3, $SrAl_2O_4$, and Al_2O_3 oxides and attractive matrices for Eu-doped phosphors. All of these findings will be described in detail in this research paper.

EXPERIMENTAL DATA

All reactions and manipulations were conducted under an atmosphere of dry N_2 using a standard Schlenk setup. The starting materials, barium (pieces, 99%), strontium (granular, 99%), $AlMe_3$ (2.0 M in toluene), ddbfoH (2,3-dihydro-2,2-dimethylbenzofuran-7-ol; 99%), and europium(III) oxide (Eu_2O_3 powder 99.9%), were obtained from Aldrich, Germany, and used as received. $InMe_3$ (2.13 M in toluene) was obtained from the Department of Chemistry at the Warsaw University of Technology. Toluene and hexanes were distilled from Na/benzophenone and P_2O_5, respectively. Infrared spectra were recorded on a Bruker 66/s FT-IR spectrophotometer in Nujol mulls. Thermogravimetric-differential thermal analyses (TGA-DTA) were recorded in a N_2 and air atmosphere on a Setaram SETSYS 16/18. NMR spectra were obtained on Bruker 300 MHz AMX and 500 MHz (Avance 500) spectrometers. GC-MS analyses were recorded on a gas chromatograph with an HP 5971A mass detector and an HP 5965B infrared detector (Hewlett-Packard). Microanalyses were conducted with an ARL model 3410 + ICP spectrometer (Fissions Instruments) and VarioEL III CHNS (in-house). Thermal decompositions were performed using an NT 1313 furnace with thermostat KXP3+ production NEOTHERM. Samples were thermolyzed in an atmosphere of air. The thermolyzed products were characterized by recording their X-ray powder diffraction (PXRD) patterns with a Bruker D8 Advance diffractometer using Cu K_α radiation (λ = 1.5418 Å). The measurements were performed for 2θ = 5−120° with 2θ step = 0.008° and a 1 s counting time. Raman spectra were recorded on a LabRam HR800 spectrophotometer. Microscope analyses were performed with a Philips SEM 515 microscope equipped with an EDAX 9800 spectrometer (30 kV, linear resolution 5 nm) and TEM FEI Tecnai G^2 20 X-TWIN. Physisorption studies were conducted using an ASAP 2020 accelerated surface area and porosimetry system. Photoluminescence spectra were recorded using an FSL920 spectrofluorometer from Edinburgh Instruments with a 450 W Xe lamp and PMT operating within a 185−870 nm range. The luminescence spectra were collected with a resolution of 0.2 nm.

$[Ba\{(\mu\text{-}ddbfo)_2InMe_2\}_2]$ (1) and $[Me_2In(\mu\text{-}ddbfo)]_2$ (2). A Schlenk flask was charged with $[Ba(ddbfoH)_4](ddbfo)_2{\cdot}ddbfoH$[36] (0.76 g; 0.59 mmol) and toluene (15 mL), and the resulting clear, colorless solution was stirred vigorously and cooled to −78 °C. A 2.13 M solution of $InMe_3$ in toluene (1.9 mL; 4.05 mmol) was then added to the mixture in a dropwise manner. Following 72 h of agitation at room temperature, workup provided two types of colorless crystals: blocks of **1** and needles of **2**. The significant differences in size and crystal morphology allowed us to isolate the two types. The crystals were separated under an atmosphere of N_2 using a Pasteur pipet. Anal. Calcd for **1**, $C_{44}H_{56}BaIn_2O_8$ (1079.89): C, 48.94; H, 5.23; Ba, 12.72. Found: C, 48.07; H, 5.20; Ba, 13.01. Anal. Calcd for **2**, $C_{24}H_{34}O_4In_2$ (616.18): C, 46.78; H, 5.57; In, 37.27. Found: C, 46.83; H, 5.56; In, 37.25. FT-IR of **1** (cm^{-1}, Nujol mull): 1878 (vw), 1698 (vw), 1610 (vs), 1590 (m), 1476 (vs), 1312 (vs), 1285 (s), 1234 (m), 1190 (m), 1164 (m), 1128 (s), 1110 (m), 1058 (m), 1034 (s), 971 (vw), 874 (s), 838 (w), 774 (s), 763 (vs), 752 (s), 721 (s), 617 (m), 598 (m), 574 (s), 539 (m), 488 (m), 468 (m), 368 (w). FT-IR of **2** (cm^{-1}, Nujol mull): 1881 (vw), 1700 (vw), 1613 (vs), 1577 (m), 1484 (vs), 1310 (vs), 1285 (s), 1231 (m), 1200 (m), 1164 (m), 1129 (s), 1111 (m), 1057 (m), 1030 (s), 965 (vw), 867 (s), 838 (w), 777 (s), 764 (vs), 750 (s), 719 (s), 621 (m), 601 (m), 574 (s), 541 (m), 491 (m). ^{1}H NMR of **1** ($C_6D_5CD_3$, 298 K): δ 6.14−5.93 (m, 3H of Ph); 2.16 (s, C$\underline{H}_2$); 0.68 (s, 2C$\underline{H}_3$); −0.21 (s, 2In−C$\underline{H}_3$). ^{13}C NMR of **1** ($C_6D_5CD_3$, 298 K): δ 148.7 (s, (C($O_{phenoxo}$))$\underline{C}$(O)), 146.7 (s, $\underline{C}(O_{phenoxo})$), 126.2 (s, C(H)$\underline{C}(CH_2)$), 122.4 (s, (CH)$\underline{C}$H(CH)), 115.8 (s, (CH)$\underline{C}$H(C)), 114.1 (s, C($O_{phenoxo}$)$\underline{C}$H(CH)), 88.5 (s, $\underline{C}(CH_3)_2$), 43.9 (s, $\underline{C}H_2$), 28.2 (s, 2C$\underline{H}_3$), −3.1 (s, 2Al-C$\underline{H}_3$). ^{1}H NMR of **2** ($C_6D_5CD_3$, 298 K): δ 7.11 − 6.58 (m, 3H of Ph), 2.44 (s, C$\underline{H}_2$), 1.02 (s, 2C$\underline{H}_3$), −0.20 (s, 2In−C$\underline{H}_3$). Purity of $BaIn_2O_4$ (%): C, 0.03; H, 0.00. EDS: Ba/In = 0.5 (±0.01). Purity of In_2O_3 (%): C, 0.00; H, 0.00. Raman (cm^{-1}) of $BaIn_2O_4$: 75 (vs), 126 (m), 192 (m), 253 (m), 304 (m), 346 (m), 378 (vw), 424 (m), 466 (vs), 551 (m), 610 (m), 680 (m), 846 (m), 992 (w). Raman (cm^{-1}) of In_2O_3: 54 (vw), 77 (w), 88 (w), 101 (m), 113 (s), 132 (vs), 162 (m), 172 (m), 187 (m), 310 (s), 369 (w), 500 (m), 633 (w).

$[Sr(ddbfoH)_4](ddbfo)_2{\cdot}ddbfoH$ (3). A Schlenk flask fitted with a reflux condenser equipped with a N_2 inlet/oil bubbler was charged with metal Sr (3.02 g; 34.47 mmol), toluene (40 mL), and 2,3-dihydro-2,2-dimethyl-7-benzofuranol (ddbfoH, 42.47 g; 258.53 mmol), and the resulting mixture was stirred at room temperature until all of the metal had been consumed (usually 3−4 h). The mixture was then filtered to give a clear, dark green solution, which was reduced in volume to approximately 25 mL. Hexanes (15 mL) were then added to the mixture, providing colorless blocks of **3** following a hold period of 72 h (30.90 g; 25.02 mmol; 73%). Anal. Calcd for **3**, $C_{70}H_{82}O_{14}Sr$ (1235.00): C, 68.07; H, 6.71; Sr, 7.09. Found: C, 68.32; H, 6.43; Sr, 7.63. FT-IR (cm^{-1}, Nujol mull): 3410 (m), 1628 (m), 1592 (m), 1460 (s), 1376 (s), 1304 (s), 1136 (s), 1066 (m), 1020 (s), 878 (s), 792 (s), 722 (s), 590 (m), 522 (m), 440 (m), 430 (m), 412 (m), 352 (m). ^{1}H NMR ($CDCl_3$, 298 K): δ 10.71 (br s, O$\underline{H}$), 7.40−6.59 (m, 3H of Ph), 2.72 (s, C$\underline{H}_2$), 1.29 (s, 2C$\underline{H}_3$). ^{13}C NMR ($CDCl_3$, 298 K): δ 148.3 (s, (C($O_{phenoxo}$))$\underline{C}$(O)), 143.7 (s, $\underline{C}(O_{phenoxo})$), 128.2 (s, C(H)$\underline{C}(CH_2)$), 122.4 (s, (CH)

dx.doi.org/10.1021/ic301218v | Inorg. Chem. 2012, 51, 9820−9832

Scheme 1. Synthesis of 1, 2, 4, and 5

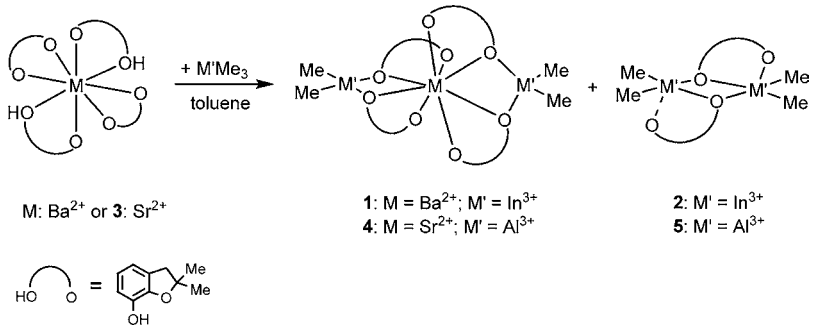

CH(CH)), 116.9 (s, (CH)CH(C)), 116.2 (s, C($O_{phenoxo}$)CH(CH)), 87.7 (s, C(CH_3)$_2$), 44.0 (s, CH_2), 28.1 (s, 2CH_3).

[Sr{(μ-ddbfo)$_2$AlMe$_2$}$_2$] (4) and [Me$_2$Al(μ-ddbfo)]$_2$ (5). A Schlenk flask was charged with **3** (0.93 g; 0.75 mmol) and toluene (15 mL), and the resulting clear, yellow-green solution was stirred vigorously and cooled to 0 °C. A 2.0 M solution of $AlMe_3$ in toluene (1.9 mL; 3.80 mmol) was then added to the mixture in a dropwise manner. The solution was warmed to room temperature, toluene (30 mL) was added, and the resulting mixture was stirred at room temperature for 24 h. The solution was then filtered, and the filtrates were reduced in volume to approximately 30 mL. Hexanes (10 mL) were then added, and the resulting mixture was cooled to −5 °C. Following a hold period of 72 h, two kinds of colorless crystals formed from within the biphasic solution, namely, blocks of **4** and needles of **5**. The significant differences in size and crystal morphology allowed us to isolate the two types. The crystals were separated under a N_2 atmosphere using a Pasteur pipet. Anal. Calcd for **4**, $C_{44}H_{56}O_8SrAl_2$ (854.50): C, 61.85; H, 6.61; Sr, 10.25; Al, 6.32. Found: C, 60.99; H, 6.93; Sr, 10.01; Al, 6.02. Anal. Calcd for **5**, $C_{24}H_{34}O_4Al_2$ (440.50): C, 65.44; H, 7.78; Al, 12.25. Found: C, 64.98; H, 7.67; Al, 12.07. FT-IR of **4** (cm^{-1}, Nujol mull): 1891 (vw), 1808 (vw), 1618 (vs), 1590 (m), 1488 (vs), 1472 (vs), 1362 (s), 1307 (vs), 1290 (s), 1234 (m), 1190 (s), 1155 (m), 1130 (s), 1111 (s), 1060 (m), 1040 (vs), 969 (w), 900 (w), 867 (s), 843 (m), 771 (vs), 717 (s), 670 (s), 587 (m), 529 (w), 500 (w), 479 (m), 373 (w). FT-IR of **5** (cm^{-1}, Nujol mull): 1889 (vw), 1812 (vw), 1617 (vs), 1590 (m), 1488 (vs), 1460 (vs), 1370 (s), 1311 (vs), 1293 (s), 1239 (m), 1190 (s), 1161 (m), 1131 (s), 1110 (s), 1055 (m), 1033 (vs), 971 (w), 903 (w), 871 (s), 842 (m), 770 (vs), 716 (s), 670 (s), 586 (m), 524 (w). ^{1}H NMR of **4** ($C_6D_5CD_3$, 298 K): δ 7.05−6.56 (m, 3H of Ph), 2.50 (s, CH_2), 1.12 (s, 2CH_3), −0.18 (s, 2Al−CH_3). ^{1}H NMR of **5** ($C_6D_5CD_3$, 298 K): δ 7.10−6.56 (m, 3H of Ph), 2.56 (s, CH_2), 1.22 (s, 2CH_3), −0.17 (s, 2Al−CH_3). Purity of $SrAl_2O_4$ (%): C, 0.04; H, 0.00. EDS: Sr/Al = 0.5 (±0.01). Purity of Al_2O_3 (%): C, 0.00; H, 0.00. Raman (cm^{-1}) of $SrAl_2O_4$: 50 (w), 90 (m), 107 (s), 114 (s), 129 (vs), 137 (m), 146 (m), 171 (m), 178 (m), 190 (w), 467 (s), 500 (w), 787 (w). Raman (cm^{-1}) of Al_2O_3: 58 (w), 78 (m), 90 (m), 103 (m), 117 (m), 128 (vs), 382 (w), 420 (m).

Oxide Preparation. In a typical procedure, the precursor was heated at the desired temperature for 5 h in air. Following decomposition, the oxide products were identified by PXRD. The morphologies and elemental compositions of $BaIn_2O_4$, In_2O_3, $SrAl_2O_4$, and Al_2O_3 particles were investigated using scanning and transmission electron microscopy equipped with an energy-dispersive spectrometer (SEM-EDS and TEM-EDS). Carbon and hydrogen contaminations following thermolysis were examined by elemental analysis. Phase purity was also confirmed by Raman spectroscopy (see Supporting Information).

Preparation of Eu-Doped Oxides. Eu-doped samples were synthesized by mixing oxides derived from **2** and **4** with Eu_2O_3, with the mixture being ground in an alumina mortar with acetone as a wetting medium. The resulting raw powder of In_2O_3:Eu^{3+} was sintered in air at 1000 °C. The Eu concentration was 3 mol % with respect to In. The raw powder of $Sr_{0.99}Eu_{0.01}Al_2O_4$ was sintered at 1300 °C under oxidizing (air) and reducing (mixture N_2−H_2 25%) atmospheres. $SrAl_2O_4$:Eu powders were also obtained using a traditional ceramic method. Stoichiometric amounts of $SrCO_3$, Al_2O_3, and Eu_2O_3 were ground with acetone and sintered at the same temperature under the same atmospheric conditions to allow for a comparison of their luminescence properties.

Details of X-ray Data Collection and Reduction. X-ray diffraction data were collected using a KUMA KM4 CCD (ω scan technique) diffractometer equipped with an Oxford Cryosystem-Cryostream cooler. The space groups were determined from systematic absences and subsequent least-squares refinement. One frame checked every 50 frames showed no crystal decay. Lorentz and polarization corrections were applied. The structures were solved by direct methods and refined by full-matrix-least-squares on F^2 using the SHELXTL package.[37] Non-hydrogen atoms were refined with anisotropic thermal parameters. Hydrogen atom positions were calculated and added to the structure factor calculations, but were not refined. Scattering factors and $\Delta f'$ and $\Delta f''$ values were taken from the literature.[38]

With the exception of structure factors, all of the data have been deposited with the Cambridge Crystallographic Data Centre (CCDC) in association with earlier communications (barium aryloxide)[31] or as supplementary publications CCDC 878064, 878065, and 878063 for **1**, **2**, and **3**. Copies of the data can be obtained free of charge by application to CCDC, 12 Union Road, Cambridge CB21EZ, UK (e-mail: deposit@ccdc.cam.ac.uk).

RESULTS AND DISCUSSION

Synthesis of Compounds 1−5. To the best of our knowledge,[26] there is a complete lack of barium−indium and strontium−aluminum species containing a M−O_{alkoxo}−M′ (M = Ba^{2+}, Sr^{2+}; M′ = In^{3+}, Al^{3+}) motif. Therefore, as an initial point of our project, we prepared the mononuclear barium 7-benzofuranoxide. The reaction of barium aryloxide [Ba(ddbfoH)$_4$]-(ddbfo)$_2$·ddbfoH[36] (ddbfoH = 2,3-dihydro-2,2-dimethyl-7-benzofuranol) with $InMe_3$ in toluene (Scheme 1) led to the abstraction of the hydroxyl protons from the cation sphere of barium and the subsequent evolution of methane MeH, as confirmed by GC/MS analysis. Consequently, the organometallic cation $InMe_2^+$ could readily coordinate to the barium anion $[Ba(ddbfo)_4]^{2-}$ core to form a heterobimetallic [Ba{(μ-ddbfo)$_2$InMe$_2$}$_2$] (**1**) aryloxo-organometallic complex. Meanwhile, the $InMe_3$ was also reacted with ddbfoH to form dimeric complex [Me$_2$In(μ-ddbfo)]$_2$ (**2**). Subsequent workup gave two kinds of colorless crystals, namely, blocks and needles of **1** and **2**, respectively, which were separated prior to any further analysis under a N_2 atmosphere using a Pasteur pipet. Such an easily performed isolation method was possible due to significant differences in size and crystal morphology. Needle-like crystals grew on the Schlenk walls, and blocks were much smaller and localized on the bottom of the flask. Unfortunately, up to now we have not been able to obtain **1** and **2** separately in the pure crystalline form.

The crystal structures of **1** and **2** were determined according to the parameters presented in Table 1 and are described in the

dx.doi.org/10.1021/ic301218v | Inorg. Chem. 2012, 51, 9820−9832

Experimental Section. Selected bond lengths and angles are outlined in Tables 2 and 3.

Table 1. Crystallographic Data for 1−3

	1	2	3
chemical formula	$5(C_{44}H_{56}BaIn_2O_8)$	$C_{24}H_{34}In_2O_4$	$C_{70}H_{82}O_{14}Sr$
fw	5399.34	616.15	1234.98
temp (K)	100(2)	100(2)	100(2)
space group	*C*2/*c*	*C*2/*c*	$P2_1/c$
a [Å]	40.809(8)	17.075(4)	20.157(5)
b [Å]	12.708(4)	9.496(3)	14.714(4)
c [Å]	42.708(9)	17.503(4)	21.812(5)
α [deg]	90.00	90.00	90
β [deg]	91.08(4)	117.41(4)	98.99(3)
γ [deg]	90.00	90.00	90
V [Å^3]	22144(9)	2519.4(15)	6390(3)
Z	4	4	4
ρ [g/cm^3]	1.620	1.624	1.299
μ(Mo K$_\alpha$) [mm^{-1}]	15.48	1.86	0.91
R1 (>2σ)	0.042	0.0202	0.039
wR2 (>2σ)	0.107	0.0456	0.066

Table 2. Selected Bond Lengths (Å) and Angles (deg) of 1

Ba(1)−O(10)	2.868(5)
Ba(1)−O(11)	2.724(4)
Ba(1)−O(20)	2.858(5)
Ba(1)−O(21)	2.733(4)
In(1)−O(11)	2.146(4)
In(1)−O(21)	2.155(4)
In(1)−C(1)	2.152(7)
In(1)−C(2)	2.171(7)
Ba(1)−O(11)−In(1)	112.10(18)
Ba(1)−O(21)−In(1)	111.46(18)

Table 3. Selected Bond Lengths (Å) and Angles (deg) for 2

In(1)−O(10)	2.641(2)
In(1)−O(11)	2.195(2)
In(1)−C(1)	2.139(2)
In(1)−C(2)	2.143(2)
O(10)−In(1)−O(11)	69.88(6)
O(10)−In(1)−C(1)	86.73(8)
O(10)−In(1)−C(2)	93.75(8)
O(11)−In(1)−C(1)	108.66(8)
O(11)−In(1)−C(2)	104.89(7)

Figure 1 presents a view of the molecular structure of **1**. The barium cation is surrounded by eight oxygen atoms from the four benzofuranoxide ligands and possesses dodecahedral geometry. The indium atoms are four-coordinate, with each of the atoms being occupied by two donor aryloxo oxygens and two carbon atoms from the methyl groups. The coordination sphere of the indium cations possesses a slightly distorted tetrahedral geometry. The Ba−O bond distances range from 2.724(4) to 2.868(5) Å, which is comparable with those observed for $[Ba\{(\mu\text{-ddbfo})_2M'Me_2\}_2]$ (M′ = Al^{3+}, Ga^{3+})[31] and other barium/group 13 heterobimetallic complexes reported in the literature.[32,39−46] The In−O distances in **1** are 2.146(4)−2.155(4) Å, and the In−C distances are 2.152(7) and 2.171(7) Å. The Ba−O−In bond angles range from 111.46(18)° to 112.10(18)°. For comparison, the Ba−O−M′ bond angles for $[Ba\{(\mu\text{-ddbfo})_2AlMe_2\}_2]$ are 109.65(8)° and 107.49(8)°, whereas they are 109.67(7)° and 111.47(7)° for $[Ba\{(\mu\text{-ddbfo})_2GaMe_2\}_2]$.[31]

The molecular structure of **2** is shown in Figure 2. Complex **2** is composed of two five-coordinate indium atoms, with each of the metal centers being surrounded by three oxygen atoms from the ddbfo$^-$ ligands and two carbon atoms from the methyl group. The indium atoms are bridged by the two aryloxo oxygens of the In_2O_2 unit, where the In−O bond distance is 2.193(2) Å. The coordination sphere of the metal centers possesses highly distorted trigonal-bipyramid geometry. Each of the In atoms lay in an equatorial plane constituted by one bridging aryloxo oxygen atom from a benzofuranoxide ligand and two carbon atoms from the methyl groups. The axial positions are occupied by an ether oxygen atom and a second aryloxo oxygen. The In−$O_{(ether)}$ bond distance is 2.641(2) Å and is much longer than the corresponding value observed in In−$O_{(alkoxo)}$. Many different suggestions have appeared in the literature regarding the nature of this bonding interaction, and an interesting analysis of this issue has been reported by Lewiński and Zachara.[47] On the basis of their studies, and by analogy with other group 13 metals,[48−51] this type of bond has been defined as a secondary or noncovalent interaction. Spectroscopic and analytical data for **1** and **2** confirmed their structural composition (see Experimental Section).

Since strontium is a technologically important ion in double oxide materials, such as spinels and perovskites,[52] in the next stage of the current studies we prepared mononuclear strontium benzofuranoxide $[Sr(ddbfoH)_4](ddbfo)_2\cdot ddbfoH$ (**3**) (ddbfoH = 2,3-dihydro-2,2-dimethylbenzofuran-7-ol). Complex **3** is air-sensitive, but could be stored for extended periods under dry N_2. This complex was obtained according to the direct reaction of metallic strontium with an excess of ddbfoH in toluene (Scheme 2).

Crystallization of **3** from a mixture of toluene and hexanes provided colorless crystals. The molecular structure of **3** (Figure 3) was determined as outlined in the Experimental Section and Table 1.

Complex **3** exists as an ionic compound with two anionic ddbfo$^-$ ligands and a neutral 7-benzofuranol outside the coordination sphere of the strontium cation. The cation and the anions are connected by hydrogen bonds, which reveal, on closer inspection, that the ddbfoH molecules have remained within the coordination sphere of strontium in the solid state. All hydrogen atoms of OH groups were clearly located from difference Fourier maps and refined without restraints. Close analysis of the O−H and O···H distances (Table 4) shows that all ligands from the metal coordination sphere keep their hydroxy hydrogens. The distances O(11)−H(11), 0.82(2); O(31)−H(31), 0.93(2); O(41)−H(41), 0.90(2); O(21)−H(61), 1.05(2); and O(71)−H(71), 0.95(2) clearly indicate the existence of O−H bonds. On the other hand, the distances O(61)···H(11), 1.78(2); O(51)···H(31), 1.55(2); O(51)···H(41), 1.58(2); O(61)···H(61), 1.41(2); and O(61)···H(71), 1.90(2) confirm that there are only intermolecular contacts. The hydrogen bonds were also found to have persisted in solution, with their presence being confirmed by the appearance of a broad singlet located at 10.71 ppm in the ^{1}H NMR spectrum. The Sr−$O_{(aryloxo)}$ bond distances range from 2.549(3) to 2.611(3) Å and are much longer than those reported for $[Sr(OPh)_8(PhOH)_2(THF)_6]$,[53] $[\{Sr_2(OMes)_2(\mu\text{-}OMes)_2(\eta^2\text{-en})(\eta^1\text{-en})(H_2O)\}(\mu\text{-en})]\cdot 3en$[54] (MesOH = 2,4,6-trimethylphenol; en = ethylenediamine), and $[Sr_2(OMes)_4(dme)_4]$[55] (dme = 1,2-dimethoxyethane), whereas

dx.doi.org/10.1021/ic301218v | Inorg. Chem. 2012, 51, 9820−9832

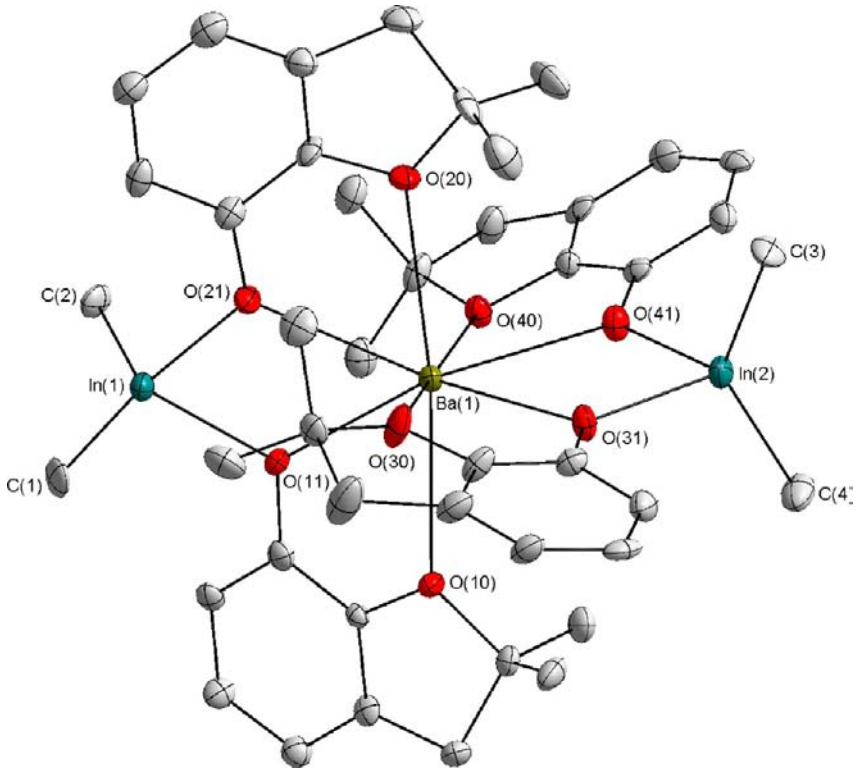

Figure 1. Molecular structure of **1** (H atoms have been omitted for clarity).

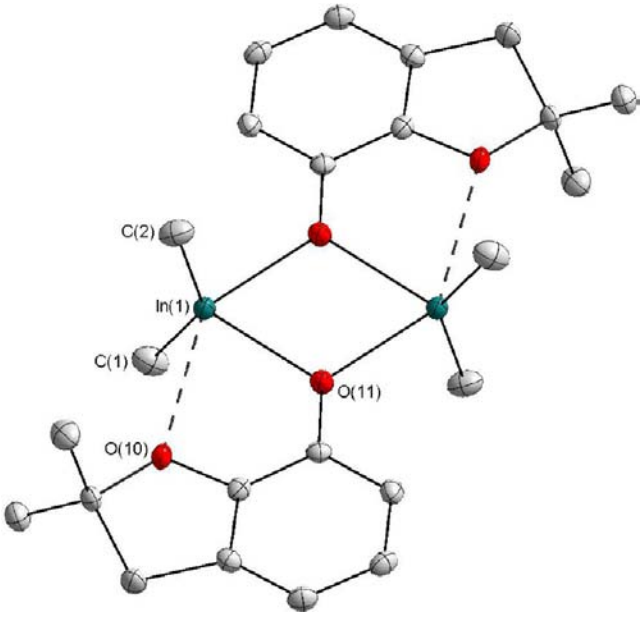

Figure 2. Molecular structure of **2** (H atoms have been omitted for clarity).

Scheme 2. Synthesis of 3

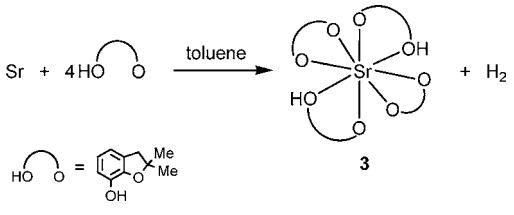

the Sr−$O_{(ether)}$ bond distances are longer than Sr−$O_{(aryloxo)}$ and range from 2.648(3) to 2.733(3) Å. The molecular structure of **3** is strongly supported by the spectroscopic data and is also similar to the structure proposed for its corresponding barium derivative.[36] It is worthy of note that, to the best of our knowledge, there are only a few examples of group 2 homoleptic alkoxide complexes in the literature. The largest group was found for barium compounds,[35,41,42,55−66] including heterometallic, molecular, and ionic complexes. A few examples have also been indentified for magnesium,[67−72] calcium,[73−78] and strontium species.[78−85]

Complex **3** was employed in a reaction with $AlMe_3$ (Scheme 1), leading to methane evolution and the linking together of ddbfo$^-$ ligands with the appropriate $AlMe_2^+$ moiety to form both $[Sr\{(\mu\text{-ddbfo})_2AlMe_2\}_2]$ (**4**) and $[Me_2Al(\mu\text{-ddbfo})]_2$ (**5**). The block- and needle-like crystals were separated according to the analogous procedure described for the mixture of **1** and **2**. Unfortunately, their crystallographic structures could not be determined completely because of the low quality of crystals obtained. In spite of this, their structures were clearly identifiable because of the resemblance to complexes **1** and **2**. These similarities were also strongly supported by the spectroscopic and elemental analysis data. For example, the signals of the aromatic protons were similar to those found for ddbfoH. Furthermore, the signals corresponding to the $AlMe_2^+$ moieties were observed at −0.18 for **4** and at −0.17 ppm for **5**. The results obtained from ^{1}H NMR analysis were also confirmed by FT-IR spectroscopy. For complex **4**, the bands at 500, 479, and 373 cm^{-1} were assigned to the ν(Sr−O) vibrational modes, and peaks at 587 and 529 cm^{-1} were characteristic of ν(Al−O) stretching vibrations. Furthermore, the ν(Al−O) bands of **5** were observed at 586 and 524 cm^{-1}. Based on spectroscopic studies, elemental analysis, and our previous investigative experience,[31] the final

dx.doi.org/10.1021/ic301218v | Inorg. Chem. 2012, 51, 9820−9832

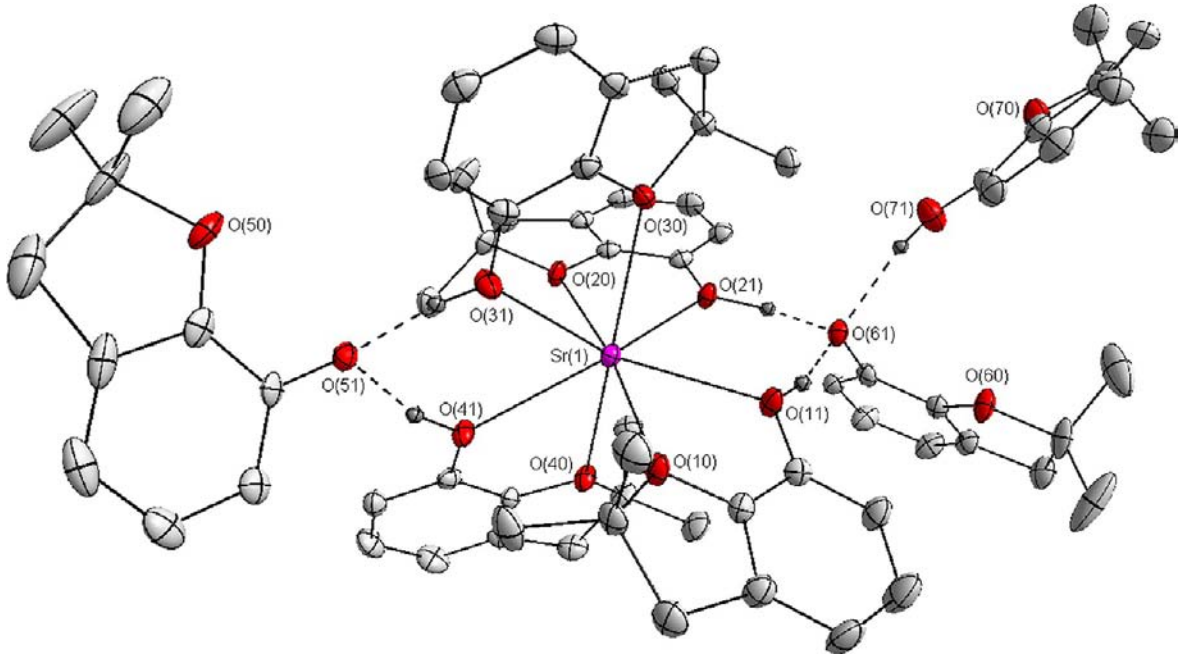

Figure 3. Molecular structure of **3** (with the exception of the hydroxyl hydrogen, the H atoms have been omitted for clarity).

Table 4. Hydrogen Bond Parameters of 3

D−H···A	D−H	H···A	D···A	∠D−H···A
O(11)−H(11)···O(61)	0.82(2)	1.78(2)	2.576(2)	163(2)
O(31)−H(31)···O(51)	0.93(2)	1.55(2)	2.462(2)	167(2)
O(41)−H(41)···O(51)	0.90(2)	1.58(2)	2.472(2)	167(2)
O(21)−H(61)···O(61)	1.05(2)	1.41(2)	2.447(2)	165(2)
O(71)−H(71)···O(61)	0.95(2)	1.90(2)	2.809(2)	158(2)

compositions of complexes **4** and **5** are proposed to be $[Sr\{(\mu\text{-ddbfo})_2AlMe_2\}_2]$ and $[Me_2Al(\mu\text{-ddbfo})]_2$, respectively.

Preparation of Oxide Materials and Their Properties. The complexes **1**, **2**, **4**, and **5** appeared to be natural molecular precursors for both spinel-like materials and group 13 oxides with compositions of type MM'_2O_4 ($M = Ba^{2+}$, Sr^{2+}; $M' = In^{3+}$, Al^{3+}) and M'_2O_3 ($M' = In^{3+}$, Al^{3+}), respectively. These compounds underwent thermal decomposition in air at the temperatures specified in Table 5. It is worthy of note that the thermal decomposition of metal alkoxides containing bulky chelating ligands was much more complex.[31] Furthermore, in comparison with metal alkoxides containing small monodentate RO^- groups (R = Me, Et, ^{i}Pr), the thermolysis process was much slower and occurred over an extended time period. This extended time period was necessary to fully decompose and remove organic contaminants from the metal oxide network. Complexes **1**, **2**, **4**, and **5** were thermolyzed for 5 h, on the basis of the phase diagrams of $BaIn_2O_4$, $SrAl_2O_4$, In_2O_3, and Al_2O_3,[86] to give phase-pure powders. The resulting materials were analyzed using microanalysis, powder X-ray diffraction, microscopy (SEM-EDS and TEM-EDS), physisorption analyses, and Raman spectroscopy.

Table 5. Thermolysis Conditions and Purity of the Resulting Oxides

precursor	temperature (°C)	product	color
1	1400	$BaIn_2O_4$	light brown
2	850	In_2O_3	light orange
4	1200	$SrAl_2O_4$	white
5	900	Al_2O_3	white

The diffraction patterns of the resulting metal oxides (Figure 4a−d) remained in agreement with those of the barium/indium $BaIn_2O_4$ and strontium/aluminum $SrAl_2O_4$ spinels and indium In_2O_3 and aluminum Al_2O_3 oxides reported in the inorganic crystal structure database (ICSD).[87] Furthermore, no residual peaks corresponding to group 2 carbonates MCO_3 ($M = Ba^{2+}$, Sr^{2+}) were observed at lower 2θ values ($2\theta < 10°$) for complexes **1** and **4**. The presence of carbonates was also excluded by elemental analysis and Fourier transform infrared spectroscopy. The phase purity of the resulting powders was confirmed using Raman spectroscopy (see Supporting Information).

Using the Debye−Scherrer equation, the average grain sizes were inter alia calculated from the PXRD spectra for the half-width of the three most intense peaks (designated on the basis of the line extending with appropriate diffractive 2θ angles: 30.7°, 31.7°, and 44.3° for $BaIn_2O_4$; 30.6°, 35.6°, and 51.5° for In_2O_3; 28.5°, 29.3°, and 35.2° for $SrAl_2O_4$; and 35.3°, 43.5°, and 57.6° for Al_2O_3 (Table 6).

The morphology and composition of the targeted oxide powders were studied by SEM-EDS/TEM-EDS. The morphologies of the desired powders are presented in Figures 5 (SEM) and 6 (TEM).

Results of the EDS analyses were consistent with the phase identification by PXRD, where spinels or group 13 oxides appeared to be the only compounds present in the samples. Standardless EDS analysis was performed for many of the grains (see Supporting Information for EDS spectra of the oxide powders examined) and confirmed the proper M:M′ ratios (Ba/In and Sr/Al = 0.5 ± 0.01). With the exception of barium, strontium, indium, aluminum, and oxygen, no other elements were detected in the samples. Only residual carbon content, from the high-purity conducting carbon tabs used to fix the powder materials, was detected during the SEM-EDS analysis. The analysis revealed irregular morphologies in the resulting metal oxides; although in the case of **2**, which was decomposed at 850

dx.doi.org/10.1021/ic301218v | Inorg. Chem. 2012, 51, 9820−9832

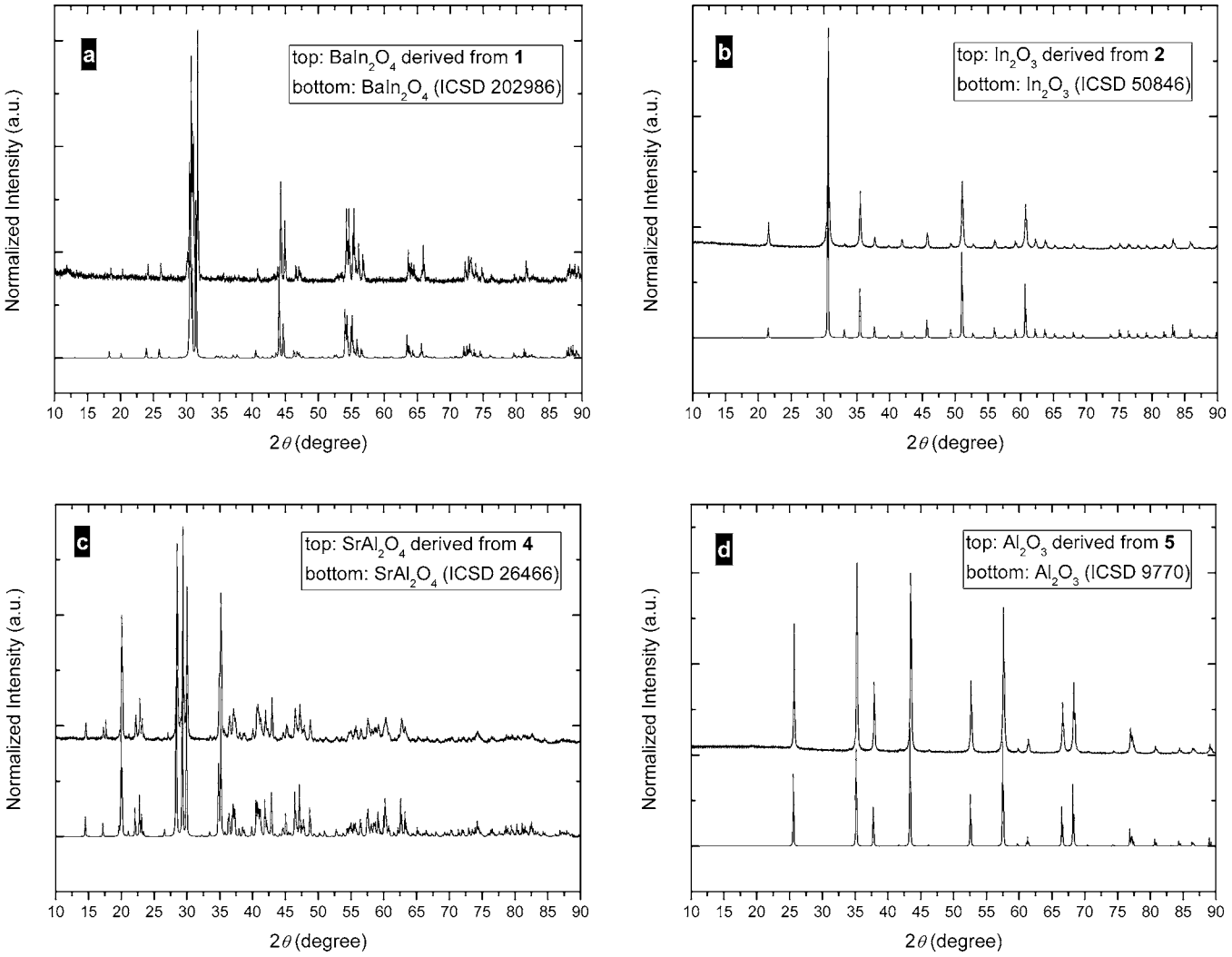

Figure 4. PXRD pattern of (a) $BaIn_2O_4$ derived from **1**, (b) In_2O_3 derived from **2**, (c) $SrAl_2O_4$ derived from **4**, and (d) Al_2O_3 derived from **5**.

Table 6. Dinitrogen Physisorption Data and Particle Size Predictions[a]

				particle size diameter [nm]	
oxide	S_{BET} [m^2/g]	$S_{Langmuir}$ [m^2/g]	δ [g/cm^3]	N_2	PXRD
$BaIn_2O_4$	0.685	1.12	6.96[88]	1258	1245−1262
In_2O_3	20.62	31.30	7.12[89]	41	38−42
$SrAl_2O_4$	2.05	3.44	3.49[90]	839	820−845
Al_2O_3	4.88	9.04	3.89[91]	316	310−325

[a]Based on the dinitrogen physisorption and PXRD data.

°C, regular diamond-shaped crystals of indium oxide were obtained (Figure 6). We are convinced that the use of other methods such as sol−gel or hydrothermal would allow for the construction of material with a certain shape and grain size. The primary aim of the current studies was to check the suitability of these molecular precursors for application in a so-called single-source strategy for obtaining highly phase-pure oxide materials with a strictly defined specific composition.

The results obtained from PXRD and SEM-EDS/TEM-EDS were further supported by Raman analysis of resulting metal oxide particles. The spectra (see Supporting Information) exhibited well-defined bands for $BaIn_2O_4$, $SrAl_2O_4$, In_2O_3, and Al_2O_3 materials in complexes **1**, **4**, **2**, and **5**, respectively. There were no traces of organic materials and no bands characteristic of the C−O vibrations of barium or strontium carbonate.

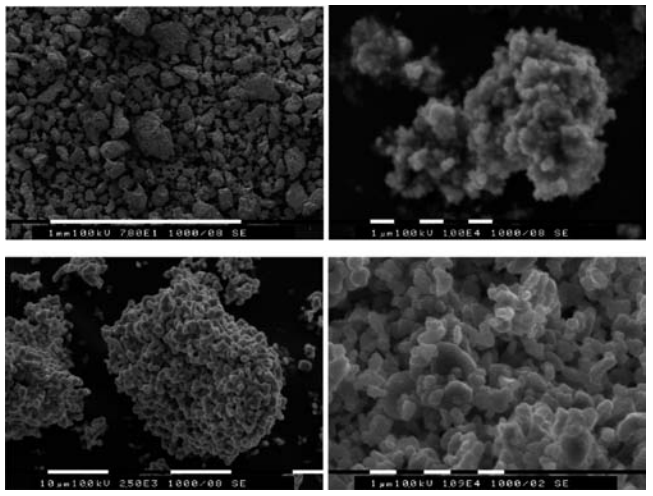

Figure 5. SEM images of (a) $BaIn_2O_4$, (b) In_2O_3, (c) $SrAl_2O_4$, and (d) Al_2O_3.

dx.doi.org/10.1021/ic301218v | Inorg. Chem. 2012, 51, 9820−9832

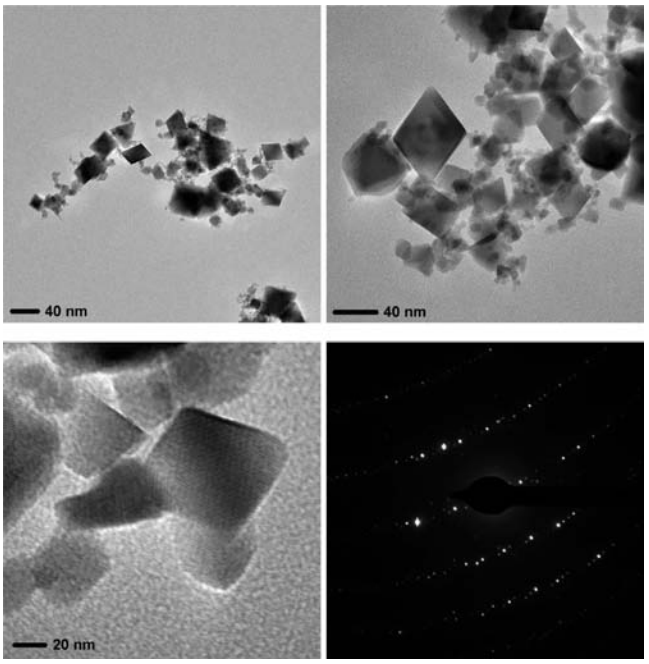

Figure 6. (a) TEM images and (b) SAED diffraction of the In_2O_3 heated at 850 °C.

Moreover, no ν(O−H) stretching bands corresponding to hydroxide aluminum or indium compounds were observed.

The nitrogen physisorption characteristics of the resulting metal oxides were examined, and the specific surface areas and total pore and micropore volumes were determined from the resulting isotherms (Figure 7a,b) (Table 6). Surface areas were measured using the Langmuir and Brunauer−Emmett−Teller (BET) models for relative pressures within $0.05 < p/p^\circ < 0.30$. The compliance of the isotherms of $SrAl_2O_4$, Al_2O_3, and $BaIn_2O_4$ with a model isotherm of α-Al_2O_3 published by Cejke et al.[92,93] showed that the resulting metal oxides were typical for materials lacking micro- and mesopores. The volume of a specific surface area was almost exclusively associated with the development of the surface as a result of the fragmentation of material on the micro- and nanoparticles.

The reduced adsorption isotherm for indium oxide deviated from the other curves in the low-pressure ranges, which suggested the presence of micropores. This was confirmed by the presence of a clear and significant hysteresis loop in the adsorption−desorption isotherm. Additional physisorption tests were therefore carried out at relative pressures in the $10^{-7} < p/p^\circ < 0.01$ range, to examine the pore size distribution. The resulting curve corresponded well with the Langmuir model. The analysis of the micropore size distribution was based on the Horvath−Kawazoe model.[94] The pore size distribution presents a single maximum (Figure 8). Micropores were present in a wide range of

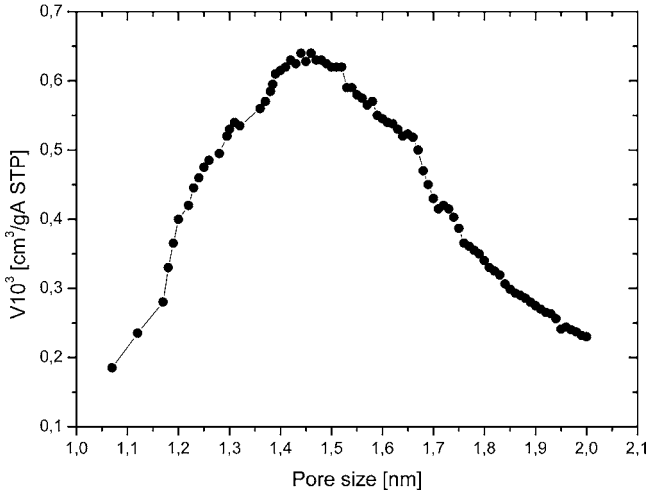

Figure 8. Micropore size distribution of In_2O_3 particles.

sizes from 1.2 to 1.8 nm, with a maximum occurring at a pore width of 1.45 nm. This suggests that the In_2O_3 nanoparticles possessed an unsettled surface because of the presence of micropores.

Luminescent Properties of a Eu-Doped $SrAl_2O_4$ Spinel and In_2O_3. Eu-doped alkaline earth aluminates have been widely studied in recent years due to their good luminescent properties such as high brightness, longevity, and chemical stability.[95−98] These phosphors have been used in a variety of applications, with examples including display devices and the lamp industry.[99,100]

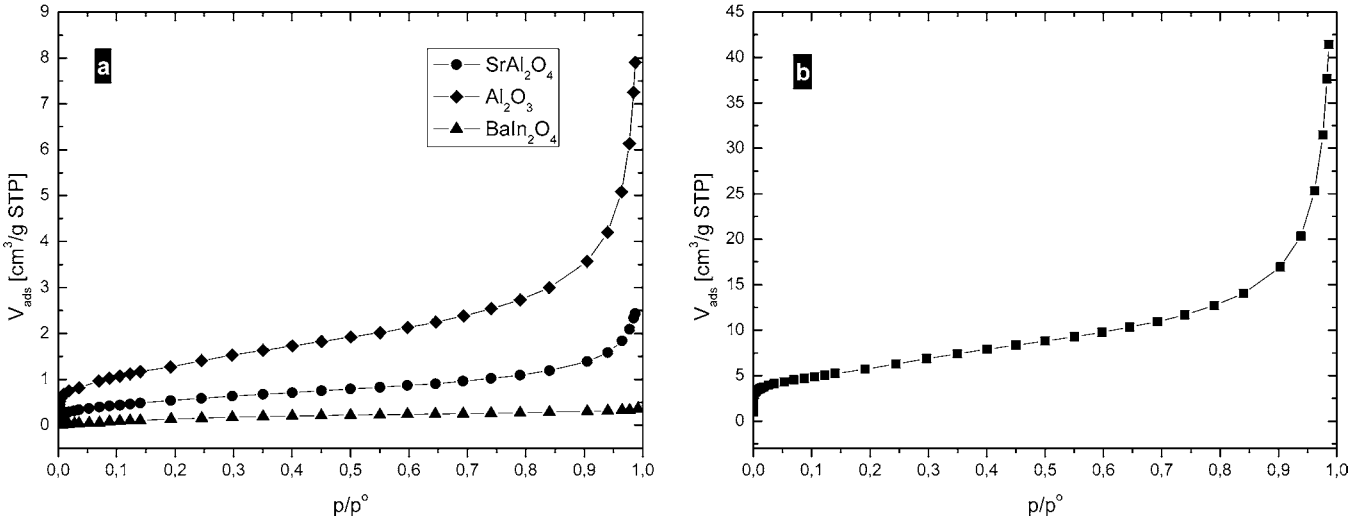

Figure 7. Adsorption isotherms of (a) $SrAl_2O_4$ (solid circles), Al_2O_3 (solid diamonds), $BaIn_2O_4$ (solid triangles), and (b) In_2O_3.

dx.doi.org/10.1021/ic301218v | Inorg. Chem. 2012, 51, 9820−9832

Eu^{2+}-activated strontium aluminate has been considered for use as a green phosphor in white light-emitting diodes (LEDs),[101] whereas $SrAl_2O_4:Eu^{3+}$ has been investigated for use as a red phosphor for LEDs.[99]

The PXRD patterns of $Sr_{0.99}Eu_{0.01}Al_2O_4$ derived from complex **4** and prepared using the solid-state method from a $SrCO_3$ and Al_2O_3 mixture are shown in Figure 9 (time of thermolysis, 10 h).

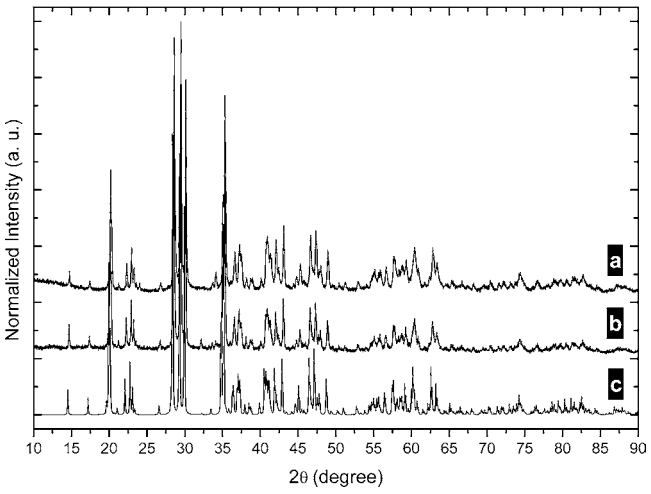

Figure 9. PXRD pattern of $Sr_{0.99}Eu_{0.01}Al_2O_4$ (a) derived from complex **4**, (b) prepared using the ceramic method, and (c) $SrAl_2O_4$ ICSD 26466.

The similar ionic radii of Eu^{2+} (0.130 nm) and Sr^{2+} (0.127 nm) and the small amount of doped ion exerted no significant influence on the structure of the host.[100] In both cases, the diffraction peaks of $SrAl_2O_4$ were in good agreement with the standard ICSD database (ICSD 26466).

Figure 10 shows the diffuse reflectance spectra of two different $SrAl_2O_4:Eu$ samples prepared by heating within two different atmospheres, namely, air and a N_2/H_2 mixture, across the spectral region from 190 to 850 nm at room temperature. The absorption spectrum of the sample sintered in a reducing (N_2 and H_2) atmosphere exhibited a broad band (peak at 350 nm)

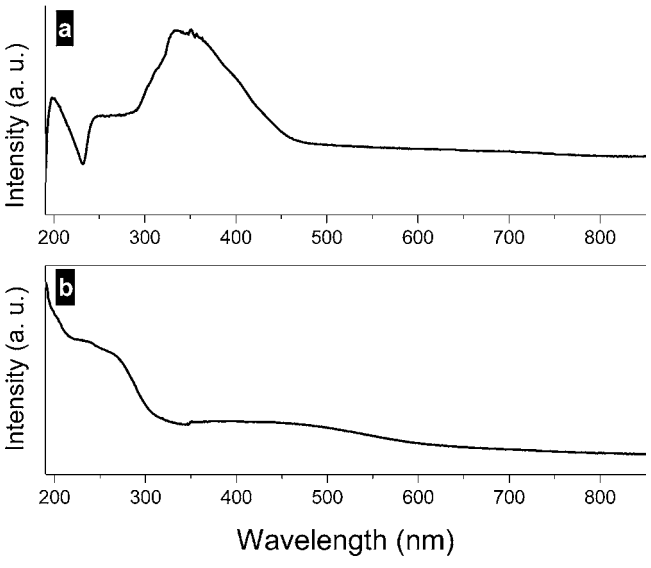

Figure 10. Absorption spectra of $Sr_{0.99}Eu_{0.01}Al_2O_4$ heated in (a) a mixture of nitrogen and hydrogen and (b) air atmosphere.

corresponding to a $4f^65d^1-4f^7$ energy level transition of Eu^{2+}. The band ranging from 230 to 270 nm was attributed to the charge transfer band (CTB) of the $Eu^{2+}-O^{2-}$ bond.[100] The energy position of this charge transfer band was closely related to the coordination number of Eu^{2+} and the covalency of the $Eu^{2+}-O^{2-}$ bond. Another band in the UV region (peak at 198 nm) was assigned to matrix absorption.[101] The absorption spectrum of the sample heated in an air atmosphere showed bands ranging from 190 to 225 nm and 230 to 300 nm, which were attributed to matrix absorption and an $Eu^{3+}-O^{2-}$ charge transfer transition, respectively. The typical 4f−4f transitions of Eu^{3+} were not observed, although a broad band was observed in the range of 350 to 550 nm.

The photoluminescence spectra of $SrAl_2O_4:Eu^{2+}$ derived from **4** are presented in Figure 11. The emission spectrum (Figure 11b) was observed as a strong green emission band, which peaked at 520 nm and was assigned to the typical $4f^65d^1-4f^7$ transition of Eu^{2+}. It is clear that the intensity of emission upon excitation at λ_{exc} = 350 nm (Eu^{2+} 4f−5d transition) was much higher than that observed upon excitation at λ_{exc} = 240 nm ($Eu^{2+}-O^{2-}$ CTB), as shown in the inset of Figure 11. The excitation spectrum (Figure 11a) corresponding to the peak at 520 nm showed an asymmetrical band (peak at 360 nm), which was attributed to the transitions from the $4f^7$ ground state to the excited state $4f^65d^1$. The asymmetry of both emission and excitation bands might be considered to be the result of different Eu^{2+} distributions in the $SrAl_2O_4$ structure. No peaks corresponding to the f−f transitions of Eu^{3+} appeared in the spectra, which confirmed that the Eu^{3+} ion has been effectively reduced to Eu^{2+} in the matrix.

Figure 12 shows the photoluminescence spectra of $SrAl_2O_4:Eu^{3+}$, which had been derived from **4** by sintering in air. The excitation spectrum of the emission at λ_{em} = 613 nm (Figure 12a) contained a series of narrow peaks in the region from 350 to 550 nm, which resulted from 4f−4f transition within the Eu^{3+} ions and originated from absorptions to the $^5D_4$ (361 nm), $^5L_7$ (380 nm), $^5L_6$ (391 nm), $^5D_3$ (412.5 nm), $^5D_2$ (462 nm), and $^5D_1$ (530 nm) states.[98] The broad band in the range from 245 to 335 nm corresponded to a charge transfer transition caused by a $Eu^{3+}-O^{2-}$ interaction. A further band, ranging from 200 to 240 nm, was observed and attributed to the host lattice absorption. The emission spectrum (Figure 12b) consisted of characteristic sharp lines, peaking at 578, 590, 613, 647, and 682 nm and attributed to the transitions from $^5D_0$ to the $^7F_0$, $^7F_1$, $^7F_2$, $^7F_3$, and $^7F_4$ levels, respectively. The most intense line was a red emission attributed to a $^5D_0-^7F_2$ electric dipole transition accompanied by the presence of a forbidden $^5D_0-^7F_0$ transition, which indicated that the local environment of the Eu^{3+} ions was not centrosymmetric. Furthermore, the high number of lines present in the spectrum suggested more than one site existed for the europium ions in the $SrAl_2O_4$ matrix. The oxidation number of the europium ions and, consequently, the photoluminescence properties of Eu-doped $SrAl_2O_4$ depended strictly on the heating atmosphere, as can be seen from the spectra (Figures 11 and 12). Sintering in air gave samples containing trivalent europium with emission in the red wavelength region, whereas sintering in a N_2/H_2 mixture provided the europium dopant as a divalent ion with emission in the green wavelength region.

The emission spectra of $Sr_{0.99}Eu_{0.01}Al_2O_4$ synthesized according to a conventional method were collected. Figure 13 shows the curves recorded and compared with the spectra of specimens derived from **4**. The emission spectra of the samples obtained according to different methods appeared similar,

dx.doi.org/10.1021/ic301218v | Inorg. Chem. 2012, 51, 9820−9832

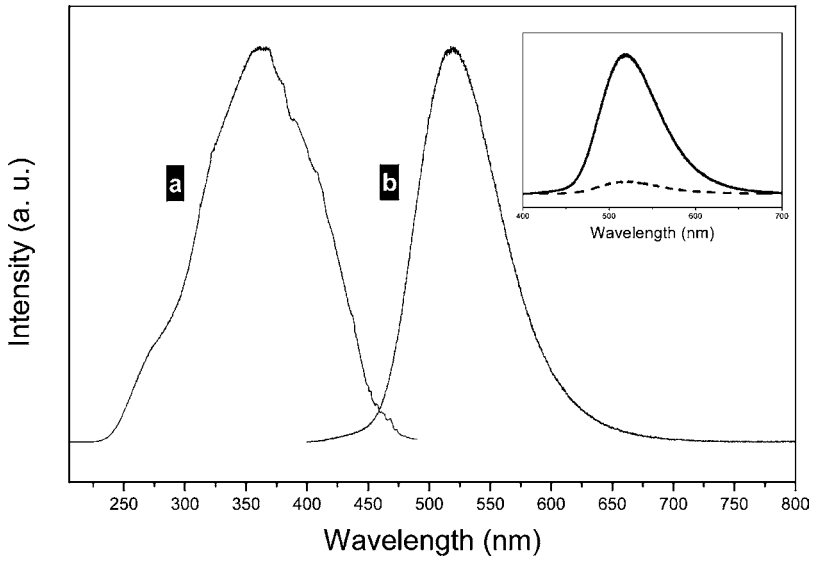

Figure 11. Photoluminescence spectra of $SrAl_2O_4:Eu^{2+}$ derived from **4**: (a) excitation spectrum (λ_{em} = 520 nm) and (b) emission spectrum (λ_{exc} = 350 nm). The inset shows emission upon excitation at 240 nm (dashed line) and 350 nm (solid line).

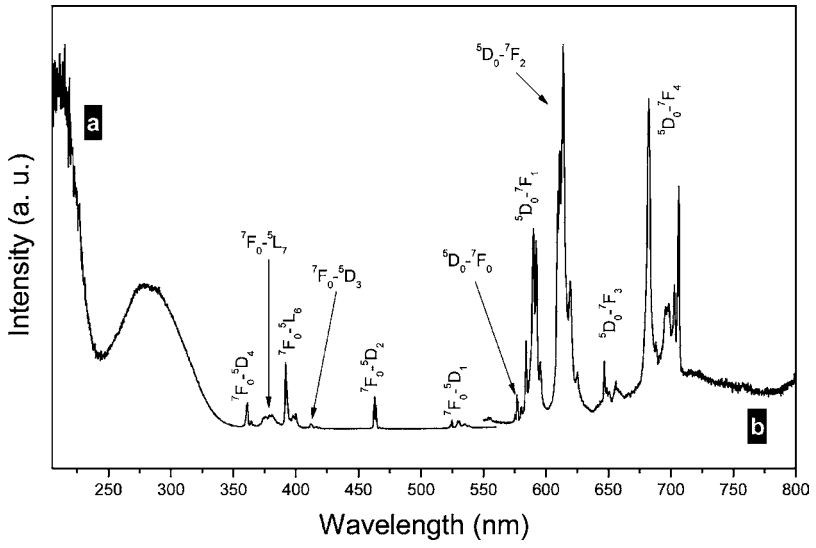

Figure 12. Photoluminescence spectra of $SrAl_2O_4:Eu^{3+}$ derived from **4**: (a) excitation spectrum (λ_{em} = 613 nm) and (b) emission spectrum (λ_{ex} = 290 nm).

although the intensity of samples derived from the molecular precursor exhibited a higher intensity. This phenomenon has also been observed for strontium aluminate doped with both divalent and trivalent europium ions.[102]

In turn, the diffuse reflectance spectra (Figure 14) of pure and Eu-doped In_2O_3 derived from **2** were characterized by similar curves. The broad absorption band was assigned to the wide band gap (3.55−3.75 eV) of indium oxide.[103] Lines corresponding to the 4f−4f transitions of Eu^{3+} were not observed.

Photoluminescence spectra for $In_2O_3:Eu^{3+}$ are shown in Figure 15. Emission peaks resulting from the transitions of the Eu^{3+} ion were not observed upon excitation at λ_{exc} = 350 nm (band gap of In_2O_3, inset in Figure 15), indicating that there was no efficient energy transfer from the host to the activator ion. Only direct excitation from the ground state $^7F_0$ to $^5D_2$ of the Eu^{3+} ion provided a series of emission peaks centered at 579.4, 585, 610.6, 649, 708, and 764 nm that contributed to the transitions from the $^5D_0$ to ^7F_J (J = 0, 1, 2, 3, 4, 5) levels of the Eu^{3+} ion, respectively (Figure 15b). The excitation spectrum (Figure 15a) was obtained by monitoring the most intensive emission of electric dipole transition $^7F_0$−$^5D_2$. It exhibited peaks located at 465 and 532 nm that were assigned to the $^7F_0$−$^5D_2$ and $^7F_0$−$^5D_1$ transitions, respectively.[104] The absence of an indium oxide host band confirmed that there was no energy transfer between the matrix and Eu^{3+} ion.

CONCLUSIONS

In conclusion, we have developed a simple synthetic approach to well-defined and previously unreported Ba−In and Sr−Al heterometallic aryloxo-organometallic complexes derived from barium or strontium 7-benzofuranoxide and trimethyl In and Al species. The corresponding indium and aluminum dimers were also isolated as byproducts from these reactions. The predesigned nature of these structures, on a molecular level, made them perfect candidates for both spinel-like and group 13 oxide nanoparticles/particles. Furthermore, these materials were

dx.doi.org/10.1021/ic301218v | Inorg. Chem. 2012, 51, 9820−9832

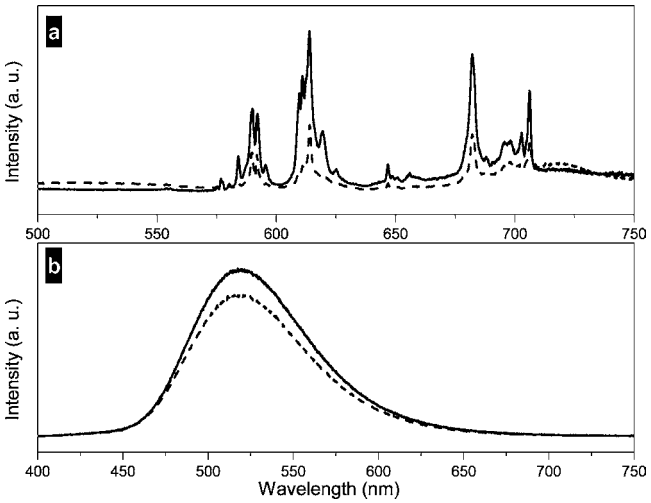

Figure 13. Comparison of the emission spectra of $Sr_{0.99}Eu_{0.01}Al_2O_4$ obtained from the molecular precursor (solid line) and the ceramic method (dashed line) sintered in (a) air and (b) N_2/H_2 mixture upon excitation at λ_{ex} = 290 nm and λ_{ex} = 350 nm, respectively.

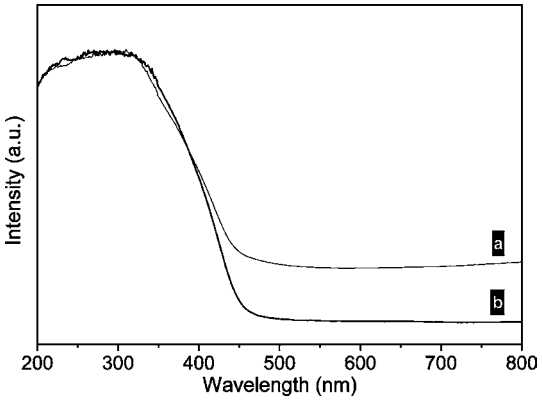

Figure 14. Absorption spectra of (a) pure and (b) Eu-doped In_2O_3.

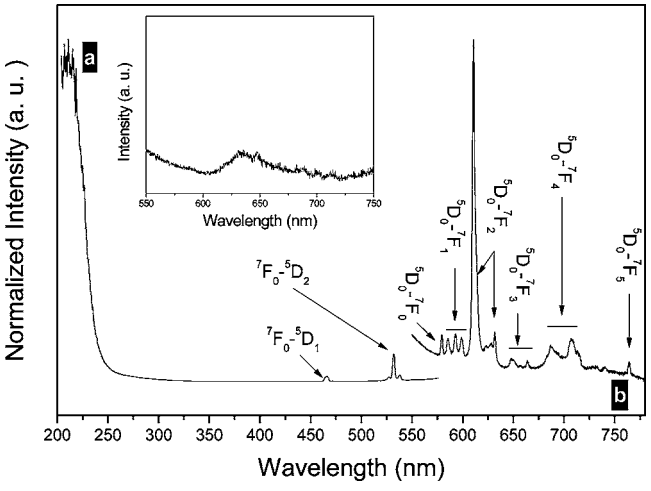

Figure 15. Photoluminescence spectra of In_2O_3:Eu^{3+}: (a) excitation spectrum (λ_{em} = 610.6 nm) and (b) emission spectrum (λ_{exc} = 465 nm). The inset shows emission upon excitation at 350 nm (band gap of In_2O_3).

constructed at relatively low temperatures according to easily controlled and highly efficient processing parameters, providing high phase purity and high yield. Our method is also attractive from an economic perspective compared to the corresponding conventional solid-state reactions using barium and strontium carbonates and an appropriate group 13 oxide, which typically require extended reaction times and high temperatures. Preliminary investigations on the Eu-doped $SrAl_2O_4$ and In_2O_3 phosphors have shown that the oxides obtained could be considered as matrices for lanthanide ions. The dependence of the luminescence properties of the Eu-doped strontium aluminates on the atmosphere employed during sintering has been investigated. An oxidizing atmosphere was shown to provide materials that emitted in the red wavelength region, whereas a reducing atmosphere afforded samples with green emission. Both phosphors were suitable candidates for applications in LED devices. Phosphors derived from the molecular precursor exhibited higher emission intensity than those obtained using the solid-state reaction. In_2O_3:Eu^{3+} showed an emission corresponding to a 4f−4f transition only after direct excitation ($^7F_0$-$^5D_2$) of the Eu^{3+} ions. There was no energy transfer between the matrix and the Eu^{3+} ions. Further studies of the luminescent properties of the obtained oxide networks are currently under way in our laboratories.

■ ASSOCIATED CONTENT

Supporting Information

Full crystallographic data, Raman spectra, EDS spectra. This material is available free of charge via the Internet at http://pubs.acs.org.

■ AUTHOR INFORMATION

Corresponding Author

*E-mail: piotr.sobota@chem.uni.wroc.pl. Tel: +48 071 375 73 06.

Notes

The authors declare no competing financial interest.

■ ACKNOWLEDGMENTS

The authors would like to express their gratitude to the National Science Centre (grant numbers: 2011/03/B/ST5/01040 and 2011/01/N/ST5/02408) for financial support. We would also like to thank Dr. Wojciech Bury and Prof. Janusz Lewiński from the Department of Chemistry at the Warsaw Technical University, for their assistance with the N_2 sorption measurements.

■ REFERENCES

(1) Hughes, R.; Sickafus, K. E. *J. Am. Ceram. Soc.* **1999**, *82*, 3277.
(2) Gallaso, F. S. *Structure and Properties of Inorganic Solids*; Pergamon: New York, 1970.
(3) Vandenberghe, R. E.; DeGrave, E. In *Mössbauer Spectroscopy Applied to Inorganic Chemistry*, Vol. 3; Long, G. J.; Grandjean, F., Ed.; Plenum: New York, 1989; p 59.
(4) Johnston, D. C.; Prakash, H.; Zachariasen, W. H.; Viswanathan, R. *Mater. Res. Bull.* **1973**, *8*, 777.
(5) McCallum, R. W.; Johnston, D. C.; Luengo, C. A.; Maples, M. P.; Low, J. *Temp. Phys.* **1976**, *25*, 177.
(6) Park, S. H.; Sun, Y.-K.; Yoon, C. S.; Kim, C.-K.; Prakash, J. *J. Mater. Chem.* **2002**, *12*, 3827.
(7) Kim, H. J.; Song, I. C.; Sim, J. H.; Kim, H.; Kim, D.; Ihm, Y. E.; Choo, W. K. *Mater. Sci. Forum* **2004**, *449−452*, 509.
(8) Gedman, N. N.; Padole, P. R.; Rithe, S. K.; Chaudhari, G. N. *J. Sol-Gel Sci. Technol.* **2009**, *50*, 296.
(9) Gaft, M.; Reisfeld, R.; Panczer, G. In *Luminescence Spectroscopy of Minerals and Materials*; Springer-Verlag: Berlin, 2005; p 96.

(10) Ye, C.; Bando, Y.; Shen, G.; Golberg, D. *Angew. Chem., Int. Ed.* **2006**, *45*, 4922.
(11) Clabau, F.; Rocquefelte, X.; Jobic, S.; Deniard, P.; Whangbo, M. H.; Garcia, A.; Le Mercier, T. *Chem. Mater.* **2005**, *17*, 3904.
(12) Holsa, J.; Aitasalo, T.; Jungner, H.; Lastusaari, M.; Niittykoski, J.; Spano, G. *J. Alloy Compd.* **2004**, *374*, 56.
(13) Holterhoff, A. G. *Am. Ceram. Soc. Bull.* **1996**, *75*, 113.
(14) Birchall, J. D.; Howard, A. J.; Kendall, K. *Nature* **1981**, *289*, 388.
(15) Yang, J.; Lin, C.; Wang, Z.; Lin, J. *Inorg. Chem.* **2006**, *45*, 8973.
(16) Gagaoudakis, E.; Bender, M.; Douloufakis, E.; Kataarakis, N.; Natsakou, N.; Cimalla, V.; Kiriakids, G. *Sens. Actuator B* **2001**, *80*, 155.
(17) Liess, M. *Thin Solid Films* **2002**, *410*, 183.
(18) Tamaki, J.; Naruo, C.; Yamanoto, Y.; Matsuoka, M. *Sens. Actuator B* **2002**, *83*, 190.
(19) Hudson, L. K.; Misra, C.; Perrotta, A. J.; Wefers, K.; Williams, F. S. *Aluminum Oxide in Ullmann's Encyclopedia of Industrial Chemistry*; Wiley-VCH: Weinheim, 2002.
(20) *GE Innovation Timeline 1957–1970.* Retrieved 2009-01-12 (http://www.docstoc.com/docs/6115980/Alumina).
(21) Vallet-Regí, M.; Colilla, M.; González, B. *Chem. Soc. Rev.* **2011**, *40*, 596.
(22) Fuji, K.; Kondo, W.; Ueno, H. *J. Am. Ceram. Soc.* **1986**, *69*, 361.
(23) Szafert, S.; John, Ł.; Sobota, P. *Dalton Trans.* **2008**, 6509.
(24) Turova, N. Y.; Turevskaya, E. P.; Kessler, V. G.; Yanovskaya, M. I. *The Chemistry of Metal Alkoxides*; Kluwer Academic Publisher: USA, 2002.
(25) Bradley, D. C.; Mehrotra, R. C.; Rothwell, I. P.; Singh, A. *Alkoxo and Aryloxo Derivatives of Metals*; Academic Press: London, 2001.
(26) *ConQuest Database* Version 1.14, CCDC, 2012.
(27) Veith, M.; Altherr, A.; Wolfanger, H. *Chem. Vap. Deposition* **1999**, *5*, 87.
(28) Seisenbaeva, G. A.; Suslova, E. V.; Kritikos, M.; Kessler, V. G.; Rapenne, L.; Andrieux, M.; Chassagneux, F.; Parola, S. *J. Mater. Chem.* **2004**, *14*, 3150.
(29) Kessler, V. G.; Seisenbaeva, G. A. *J. Sol-Gel Sci. Technol.* **2004**, *31*, 63.
(30) Utko, J.; Ejfler, J.; Szafert, S.; John, Ł.; Jerzykiewicz, L. B.; Sobota, P. *Inorg. Chem.* **2006**, *45*, 5302.
(31) John, Ł.; Utko, J.; Szafert, S.; Jerzykiewicz, L. B.; Kępiński, L.; Sobota, P. *Chem. Mater.* **2008**, *20*, 4231.
(32) Drąg-Jarząbek, A.; Kosińska, M.; John, Ł.; Jerzykiewicz, L. B.; Sobota, P. *Chem. Mater.* **2011**, *23*, 4212.
(33) Sobota, P.; Drąg-Jarząbek, A.; John, Ł.; Utko, J.; Jerzykiewicz, L. B.; Duczmal, M. *Inorg. Chem.* **2009**, *48*, 6584.
(34) Sobota, P.; Utko, J.; John, Ł.; Jerzykiewicz, L. B.; Drąg-Jarząbek, A. *Inorg. Chem.* **2008**, *47*, 7939.
(35) Westerhausen, M. *Dalton Trans.* **2006**, 4755.
(36) Utko, J.; Szafert, S.; Jerzykiewicz, L. B.; Sobota, P. *Inorg. Chem.* **2005**, *44*, 5194.
(37) *SHELXTL*, Version 6.14; Bruker AXS Inc.: Madison, WI, USA, 2003.
(38) Kromer, D. T.; Waber, J. T. In *International Tables for X-ray Crystallography*; Ibers, J. A.; Hamilton, W. C., Eds.; Kynoch: Birmingham, U.K., 1974; Vol. *4*, pp 72–98, 149–150; Tables 2.2B and 2.3.1.
(39) Zuniga, M. F.; Deacon, G. B.; Ruhlandt-Senge, K. *Chem.—Eur. J.* **2007**, *13*, 1921.
(40) Labrize, F.; Hubert-Pfalzgraf, L. G.; Daran, J.-C.; Halut, S.; Tobaly, P. *Polyhedron* **1996**, *15*, 2707.
(41) Petrella, A. J.; Roberts, N. K.; Craig, D. C.; Raston, C. L.; Lamb, R. N. *Chem. Commun.* **2003**, 2288.
(42) Deacon, G. B.; Forsyth, C. M.; Junk, P. C. *J. Organomet. Chem.* **2000**, *607*, 112.
(43) Veith, M.; Mathur, S.; Huch, V. *Inorg. Chem.* **1997**, *36*, 2391.
(44) Veith, M.; Mathur, S.; Huch, V.; Decker, T. *Eur. J. Inorg. Chem.* **1998**, 1327.
(45) Petrella, A. J.; Craig, D. C.; Lamb, R. N.; Raston, C. L.; Roberts, N. K. *J. Chem. Soc., Dalton Trans.* **2004**, 327.
(46) Guillemot, G.; Solari, E.; Rizzoli, C.; Floriani, C. *Chem.—Eur. J.* **2002**, *8*, 2072.
(47) Lewiński, J.; Zachara, J.; Justyniak, I. *Chem. Commun.* **2002**, 1586.
(48) Lewiński, J.; Zachara, J.; Justyniak, I. *Chem. Commun.* **1997**, 1519.
(49) Francis, J. A.; McMahon, N.; Bott, S. G.; Barron, A. R. *Organometallics* **1999**, *18*, 4399.
(50) Lewiński, J.; Justyniak, I.; Ochal, Z.; Zachara, J. *J. Chem. Soc., Dalton Trans.* **1999**, 2909.
(51) Schumann, H.; Frick, M.; Heymer, B.; Girgsdies, F. *J. Organomet. Chem.* **1996**, *512*, 117.
(52) Szot, K.; Speier, W.; Bihlmayer, G.; Waser, R. *Nat. Mater.* **2006**, *5*, 312.
(53) Drake, S. R.; Streib, W. E.; Chisholm, M. H.; Carlton, K. G. *Inorg. Chem.* **1990**, *29*, 2707.
(54) Teng, W.; Guino, M.; Hitzbleck, J.; Englich, U.; Ruhlandt-Senge, K. *Inorg. Chem.* **2006**, *45*, 9531.
(55) Deacon, G. B.; Junk, P. C.; Moxey, G. J.; Guino-o, M.; Ruhlandt-Senge, K. *Dalton Trans.* **2009**, 4878.
(56) Koferstein, R.; Jager, L.; Lorenz, V.; Abicht, H.-P.; Woltersdorf, J.; Pippel, E.; Görls, H. *Solid State Sci.* **2005**, *7*, 1280.
(57) Jager, L.; Lorenz, V.; Muller, T.; Abicht, H.-P.; Rossel, M.; Görls, H. *Z. Anorg. Allg. Chem.* **2004**, *630*, 189.
(58) Zhang, J.; Hubert-Pfalzgraf, L. G.; Luneau, D. *Polyhedron* **2005**, *24*, 1185.
(59) Poncelet, O.; Hubert-Pfalzgraf, L. G.; Toupet, L.; Daran, J. C. *Polyhedron* **1991**, *10*, 2045.
(60) Borup, B.; Streib, W. E.; Caulton, K. G. *Chem. Ber.* **1996**, *129*, 1003.
(61) Caulton, K. G.; Chisholm, M. H.; Drake, S. R.; Folting, K. *Inorg. Chem.* **1991**, *30*, 1500.
(62) Bhavan, R.; Hancock, R. D.; Wade, P. W.; Boyens, J. C. A.; Dobson, S. M. *Inorg. Chim. Acta* **1990**, *171*, 235.
(63) Borup, B.; Samuels, J. A.; Streib, W. E.; Caulton, K. G. *Inorg. Chem.* **1994**, *33*, 994.
(64) Boulmaaz, S.; Papiernik, R.; Hubert-Pfalzgraf, L. G.; Daran, J. C. *Eur. J. Solid State Inorg. Chem.* **1993**, *30*, 583.
(65) Yanovsky, A. I.; Turevskaya, E. P.; Yanovskaya, M. I.; Kessler, V. G.; Turova, N. Ya.; Pisarevskii, A. P.; Struchkov, Yu. T. *Zh. Neorg. Khim.* **1995**, *40*, 355.
(66) Deacon, G. B.; Junk, P. C.; Moxey, G. J.; Ruhlandt-Senge, K.; St. Prix, C.; Zuniga, M. F. *Chem.—Eur. J.* **2009**, *15*, 5503.
(67) Valle, G.; Baruzzi, G.; Paganetto, G.; Depaoli, G.; Zannetti, R.; Marigo, A. *Inorg. Chim. Acta* **1989**, *156*, 157.
(68) Sassmannshausen, J.; Riedel, R.; Pflanz, K. B.; Chmiel, H. *Z. Naturforsch., B: Chem. Sci.* **1993**, *48*, 7.
(69) Jones, A. C.; Davies, H. O.; Leedham, T. J.; Wright, P. J.; Crosbie, M. J.; Steiner, A.; Bickley, J. F.; O'Brien, P.; White, A. J. P.; Williams, D. J. *J. Mater. Chem.* **2001**, *11*, 544.
(70) Starikova, Z. A.; Yanovsky, A. I.; Turevskaya, E. P.; Turova, N. Ya. *Polyhedron* **1997**, *16*, 967.
(71) Yanovsky, A. I.; Starikova, Z. A.; Turova, N. Ya.; Chebukov, D. E.; Turevskaya, E. P. *Zh. Neorg. Khim.* **2002**, *47*, 1800.
(72) Thomas, H.; Epple, M.; Viebrock, H.; Reller, A. *J. Mater. Chem.* **1995**, *5*, 589.
(73) Goel, S. C.; Matchett, M. A.; Chiang, M. Y.; Buhro, W. E. *J. Am. Chem. Soc.* **1991**, *113*, 1844.
(74) Rogers, R. D.; Bond, A. H. *Acta Crystallogr., Sect. C: Cryst. Struct. Commun.* **1992**, *48*, 1782.
(75) Odoko, M.; Yamamoto, K.; Okabe, N. *Acta Crystallogr., Sect. C: Cryst. Struct. Commun.* **2002**, *58*, 469.
(76) Junk, P. C. *J. Chem. Crystallogr.* **1999**, *29*, 997.
(77) Hundal, G.; Martinez-Ripoll, M.; Hundal, M. S.; Poonia, N. S. *Acta Crystallogr., Sect. C: Cryst. Struct. Commun.* **1996**, *52*, 789.
(78) Zuniga, M. F.; Deacon, G. B.; Ruhlandt-Senge, K. *Inorg. Chem.* **2008**, *47*, 4669.
(79) Kazak, C.; Hamamci, S.; Topcu, Y.; Yilmaz, V. T. *J. Mol. Struct.* **2003**, *657*, 351.
(80) Camacho-Camacho, C.; Merino, G.; Martinez-Martinez, F. J.; Noth, H.; Contreras, R. *Eur. J. Inorg. Chem.* **1999**, 1021.

(81) Taeb, A.; Krischner, H.; Kratky, C. *Z. Kristallogr.* **1986**, *177*, 263.
(82) Baxter, I.; Drake, S. R.; Hursthouse, M. B.; Malik, K. M. A.; Mingos, D. M. P.; Plakatouras, J. C.; Otway, D. J. *Polyhedron* **1998**, *17*, 625.
(83) Jones, A. C.; Davies, H. O.; Leedham, T. J.; Wright, P. J.; Crosbie, M. J.; Steiner, A.; Bickley, J. F.; O'Brien, P.; White, A. J. P.; Williams, D. J. *J. Mater. Chem.* **2001**, *11*, 544.
(84) Poonia, N. S.; Chhabra, N.; Sheldrick, W. S.; Hundal, G.; Obrai, S.; Hundal, M. S. *Acta Crystallogr., Sect. C: Cryst. Struct. Commun.* **1999**, *55*, 24.
(85) Rogers, R. D.; Jezl, M. L.; Bauer, C. B. *Inorg. Chem.* **1994**, *33*, 5682.
(86) *Golden Book of Phase Transitions*; Wroclaw, 2002; p 1.
(87) *Inorganic Crystal Structure Database—ICSD*, Version 1.4.2; 2007-2.
(88) Lalla, A.; Mueller-Buschbaum, H. *J. Less-Common Met.* **1989**, *154*, 233.
(89) Nadaud, N.; Lequeux, N.; Nanot, M.; Jove, J.; Roisnel, T. *J. Solid State Chem.* **1998**, *135*, 140.
(90) Fukuda, K.; Fukushima, K. *J. Solid State Chem.* **2005**, *178*, 2709.
(91) Novoselova, T.; Malinov, S.; Sha, W.; Zhecheva, A. *Mat. Sci. Eng.* **2004**, *371*, 103.
(92) Cejka, J.; Zilkova, N.; Rathousky, J.; Zukal, A.; Jagiełło, J. *Langmuir* **2004**, *20*, 7532.
(93) Cejka, J.; Zilkova, N.; Rathousky, J.; Zukal, A. *Phys. Chem. Chem. Phys.* **2001**, *3*, 5076.
(94) Horvath, G.; Kawazoe, K. *J. Chem. Eng. Jpn.* **1983**, *16*, 470.
(95) Fu, Z.; Zhou, S.; Yu, Y.; Zhang, S. *Chem. Phys. Lett.* **2009**, *355*, 2491.
(96) Qiang, R. F.; Xiao, S.; Ding, J. W.; Yuan, W.; Zhu, C. *J. Lumin.* **2009**, *129*, 826.
(97) Choi, S. H.; Kim, N. H.; Yun, Y. H.; Choi, S. C. *J. Ceram. Process. Res.* **2006**, *7*, 62.
(98) Wu, Z. C.; Shi, J. X.; Wang, J.; Wu, H.; Su, Q.; Gong, M. L. *Mater. Lett.* **2006**, *60*, 3499.
(99) Singh, V.; Zhu, J. J.; Tiwari, M.; Soni, M.; Aynayas, M.; Hyun, S. H.; Narayanan, R.; Mohapatra, M.; Natarajan, V. *J. Non-Cryst. Solids* **2009**, *355*, 2491.
(100) Yu, X.; Zhou, C.; He, X.; Peng, Z.; Yang, S. P. *Mater. Lett.* **2004**, *58*, 1087.
(101) Cordoncillo, E.; Julian-Lopez, B.; Martinez, M.; Sanjuan, M. L.; Escribano, P. *J. Alloys Compd.* **2009**, *484*, 693.
(102) Blasse, G.; Grabmeier, B. C. *Luminescent Materials*; Springer—Verlag: Berlin, 1994.
(103) Murali, A.; Barve, A.; Leppert, V. J.; Risbud, S. H. *Nano Lett.* **2001**, *1*, 287.
(104) Xiao, Q.; Liu, Y.; Liu, L.; Li, R.; Luo, W.; Chen, X. *J. Phys. Chem. C* **2010**, *114*, 9314.